# Multiple-quantum dynamics in NMR: A directed walk through Liouville space

Michael Munowitz
*Amoco Research Center, P. O. Box 400, Naperville, Illinois 60566*

Alexander Pines
*Chemistry Department, University of California and Materials and Molecular Research Division, Lawrence Berkeley Laboratory, Berkeley, California 94720*

Michael Mehring
*2. Physikalisches Institut, Universität Stuttgart, Pfaffenwaldring 57, D-7000 Stuttgart 80, West Germany*

(Received 3 October 1986; accepted 2 December 1986)

An approach to spin dynamics in systems with many degrees of freedom, based on a recognition of the constraints common to all large systems, is developed and used to study the excitation of multiple-quantum coherence under a nonsecular dipolar Hamiltonian. The exact equation of motion is replaced by a set of coupled rate equations whose exponential solutions reflect the severe damping expected when many closely spaced frequency components are superposed. In this model the evolution of multiple-quantum coherence under any bilinear Hamiltonian is treated as a succession of discrete hops in Liouville space, with each hop taking the system from a $K$-spin/$n$-quantum mode to a $K'$-spin/$n'$-quantum mode. In particular, for a pure double-quantum Hamiltonian the selection rules are $\Delta K = \pm 1$ and $\Delta n = \pm 2$. The rate for each move depends on the number of Liouville states at the origin and destination, and on the total number of spins present. All rates are scaled uniformly by a factor dependent on the properties of the material, such as the dipolar linewidth, but otherwise the behavior predicted is universal for all sufficiently complicated systems. Results derived by this generic approach are compared to existing multiple-quantum data obtained from solids and liquid crystals.

## I. INTRODUCTION

A complete description of $N$ coupled spin-1/2 nuclei is provided by a density operator composed of $2^{2N}$ orthogonal components, each representing an independent degree of freedom and each carrying with it some particular physical significance.[1] When expressed in terms of single-spin angular momentum operators, an eigenoperator associated with a given degree of freedom may be classified first according to the number of spins correlated out of the total set and then according to the difference in Zeeman quantum numbers for each pair of states connected by a nonzero matrix element.[2] Of the various combinations, however, only a limited number are either single-spin/single-quantum operators, corresponding to components of transverse magnetization, or single-spin/zero-quantum operators, corresponding to components of longitudinal magnetization. The remaining degrees of freedom generally pertain to multiple-spin/multiple-quantum modes, which, although not directly observable in Fourier transform NMR, may be excited nevertheless and monitored indirectly in two-dimensional experiments.[3] Coherences of this sort now are routinely created and manipulated in a large number of time-domain NMR methods, where their properties are used to shape the dynamical evolution of the system, often to engineer some form of selective excitation or to control the spectral response. Examples of such methods include various techniques designed to identify subsystems with selected groupings of spins or coupling patterns as well as techniques designed to establish networks of correlated spins through coherence transfer.[4]

Multiple-quantum dynamics are clearly understood in isotropic phases, where the scalar, or $J$, coupling is the principal mechanism for spin–spin interactions. When the differences in chemical shifts are sufficiently large compared to the coupling constants, the coupling effectively reduces to a weak form in which the $z$ component of spin angular momentum is separately quantized for each spin. Under these circumstances the Hamiltonian is a sum of commuting terms, so there exists no way for two spins to exchange energy by a conservative "flip–flop" process. As a result, the dynamics are simplified to the point where the equation of motion can be solved analytically regardless of the number of spins involved.[2]

The situation is far more complex in solids and anisotropic fluids, however, for there the direct dipole–dipole couplings, typically strong, usually determine the development of the system with time.[5–12] Analytic solutions are possible only for very small systems once strong coupling is introduced, and soon even numerical solutions become impossible owing to the huge numbers of degrees of freedom that must be considered. For example, the dimension of the density operator grows from 4096 when $N = 6$ to $4.4\times10^{12}$ when $N = 21$, and to $1.6\times10^{60}$ when $N = 100$. These large numbers notwithstanding, the ability to model multiple-quantum dynamics, even approximately, under a strong-coupling Hamiltonian is worth developing, for recent experiments have demonstrated that coherences of high order can be observed in solids and liquid crystals.[9–12] Analysis of the development of multiple-quantum coherence in these systems with increasing excitation time has shown that dilute clusters of nuclei can be identified and studied, thereby

 0021-9606/87/063172-11$02.10 

suggesting a potentially new and important role for multiple-quantum NMR in the area of materials characterization.[11–14]

Despite the complexity of a large system, or perhaps because of it, on the macroscopic level there may yet appear a pattern of behavior simple enough to predict with a model that neglects the complicated internal details. This principle, which underlies all thermodynamic treatments, frequently applies to magnetic resonance phenomena involving large numbers of spins. For example, in a rigid solid the $^1$H magnetization observed after a $\pi/2$ pulse appears to decay monotonically, although the free induction signal contains frequency components distributed quasicontinuously over a broad range. The simple overall response results from the interference of the different frequencies, a phenomenon which masks the oscillations and eventually damps out the signal, giving rise to a broad, featureless spectrum in the frequency domain.[15] Consequently, except for the linewidths, the general appearance of the $^1$H NMR spectra obtained from most dipolar solids may be readily predicted just by recognizing the constraints imposed by the size of the system. Similar constraints may be expected to govern other aspects of the dynamics of large systems as well, in particular the excitation of multiple-quantum coherence under a nonsecular Hamiltonian. With this view in mind, we seek to formulate a simple model for multiple-quantum dynamics in the presence of strong coupling, through which may emerge certain features common to all systems.

The picture developed in this article approaches these goals first by defining the portion of Liouville space relevant to multiple-quantum phenomena, and then by treating the dynamical evolution as a series of discrete hops in the reduced space. The rate and terminal point of each hop are controlled by the degeneracies of the coherences involved and by the Hamiltonian governing the system, with the dipolar linewidth establishing a basic rate of flow. In this way we are able to examine the development of $n$-quantum coherence in systems of increasing size and to compare these generic results to experimental data already published for specific systems.

## II. THEORY

### A. Exact formulation of multiple-quantum dynamics in Liouville space

The assembly of $N$ spins, represented formally by a density operator $\rho$, develops in time according to the Liouville–von Neumann equation,

$$\frac{d\rho}{dt} = i[\rho, H] , \tag{1}$$

where $H$ is the internal Hamiltonian in the rotating frame. Since any operator for the system may be constructed from a complete set of orthonormal basis operators, the density operator is alternatively viewed as a *vector* in Liouville space,[16] given by

$$|\rho(t)) = \sum_{K=0}^{N} \sum_{n=-K}^{K} \sum_{p} g_{Knp}(t) |Knp) . \tag{2}$$

Each Liouville ket $|Knp)$ in this expression represents a basis operator in which $K$ single-spin angular momentum operators form a product that connects Zeeman states differing by $n$ units. (Note that we specifically use the symbol $|\cdots)$, rather than $|\cdots\rangle$, in order to distinguish Liouville states from Hilbert states.) The label $p$ associated with the operator is an additional index needed to keep track of the different ways of realizing the same values of $K$ and $n$. If we denote the spin angular momentum operator $I_\alpha$ for a spin with index $s_j$ by a ket $|s_j\alpha_j)$, then we may write a particular basis operator as

$$|Knp) = |s_1\alpha_1)|s_2\alpha_2)\cdots|s_K\alpha_K) , \tag{3}$$

taking $n$, the order of the $K$-spin coherence, as the algebraic sum of the components $\alpha(=1, 0, -1$ or, equivalently, $+, z, -)$ for each spin. For example, there are six two-spin, one-quantum operators possible in a system of three spins: $I_{1+}I_{2z}$, $I_{1z}I_{2+}$, $I_{1+}I_{3z}$, $I_{1z}I_{3+}$, $I_{2+}I_{3z}$, and $I_{2z}I_{3+}$. Each of these operators is represented in Liouville space by a ket $|Knp)$ in which $K=2$, $n=+1$, and $p$ runs from 1 through 6. In addition, the states $|Knp)$ may be normalized so that their scalar products $(Knp|Knp)$, related to traces in Hilbert space, are equal to unity. Details and definitions pertaining to the Liouville states and their matrix elements are provided in Appendix A.

The equation of motion now may be recast as a vector equation

$$\frac{d}{dt}|\rho(t)) = -i\hat{H}|\rho(t)) , \tag{4}$$

where $\hat{H}$ is a superoperator, defined by

$$\hat{H} = [H,\ldots] . \tag{5}$$

Expressed in terms of the components $g_{Knp}$, this equation is given by the equivalent set

$$\frac{d}{dt} g_{Knp}(t) = -i \sum_{K'} \sum_{n'} \sum_{p'} \Omega_{Knp;K'n'p'} g_{K'n'p'}(t) , \tag{6}$$

with

$$g_{Knp}(t) = \frac{(Knp|\rho(t))}{(Knp|Knp)} \tag{7}$$

and

$$\Omega_{Knp;K'n'p'} = \frac{(Knp|\hat{H}|K'n'p')}{(Knp|Knp)} . \tag{8}$$

Thus the behavior of even the most complex systems can be described formally and exactly, but with deceptive simplicity, by a set of coupled differential equations. In principle, the future development of the system is known once the initial condition $\rho(0)$ and the Hamiltonian are specified. Yet knowledge of both the initial condition, usually Zeeman order, and the Hamiltonian, which follows from knowledge of the internal interactions and rf pulses present during the excitation period, cannot guarantee an exact solution. Since such a solution is not within reach for large strongly coupled systems, we therefore need to replace the exact density operator formalism with a picture that retains the important physical features while reducing the mathematical complexity.

### B. Hopping model

Although Eqs. (6) suggest that the various components of the density operator should vary sinusoidally with time, such oscillations are unlikely to be apparent in systems large enough to exhibit interference of the sort discussed in the introduction. If, for example, the conventional free induction signal decays monotonically to yield a spectrum with no fine structure, then we may reasonably expect that the development of multiple-quantum signals will be similarly damped. This assumption is justified by realizing that, except for coherences of the highest order (where $n = N$ or perhaps $n = N - 1$), the dynamical evolution of all degrees of freedom will be determined by frequencies too numerous and too close together to be distinguished.[17] Hence, in anticipation of the most physically reasonable result, we will seek to replace the exact equation of motion for the density operator with a set such as

$$\frac{d\mathbf{g}}{dt} = \mathbf{R}\mathbf{g}\,, \tag{9}$$

whose solutions are exponential, not oscillatory. In this new picture, $\mathbf{g}(t)$ is a multidimensional vector formed by the coefficients of $|\rho(t))$, and $\mathbf{R}$ is a matrix of real numbers where each element is a measure of the rate of change from one component of $\mathbf{g}(t)$ to another. The formulation is equivalent to a multisite exchange, or hopping, model; the question now is to define the space over which the coherences "hop" and to develop the rates and selection rules that govern the motion.

#### 1. Selection rules

Eventually we will treat all coherences $|Knp)$ as equivalent and just use the quantum numbers $K$ and $n$. Accordingly, a simplified picture of the relevant portion of Liouville space may be obtained by projecting the whole of the space onto the $K$–$n$ plane, as in Fig. 1. What remains is a two-dimensional grid in which each point denotes a family of coherences (or basis operators) $|Kn)$, with $K \geqslant 1$ and $n = K, K-1, \ldots, 0, \ldots, -K$. In this way the number of operators that must be considered is reduced from $2^{2N}$ to a figure on the order of $N$.

The specific points in Liouville space accessible to the system are determined by the Hamiltonian, through the scalar products $\Omega_{Knp;K'n'p'}$ defined above in Eq. (8). In general, the interactions will be described by $K$-spin, $n$-quantum operators of various orders, but for multiple-quantum coherence to emerge the spins must develop under a nonsecular Hamiltonian that is at least bilinear in the spin angular momentum operator. The properties of several two-spin Hamiltonians are discussed in Appendix B, but for now we choose the double-quantum Hamiltonian

$$H_{yx} = -\frac{1}{2}\sum_{j<k} D_{jk}(I_{+j}I_{+k} + I_{-j}I_{-k}) \equiv \Sigma D_{jk}H_{jk} \tag{10}$$

used previously in experimental studies of multiple-quantum phenomena in solids and anisotropic fluids,[6,9] to make the treatment concrete. In practice, this form of the dipolar coupling usually is obtained as an average Hamiltonian, typically over a cycle of eight rf pulses. Note that $H_{yx}$ is related to the secular dipolar interaction $H_{zz}$ as

$$H_{yx} = \tfrac{1}{3}(H_{yy} - H_{xx})\,, \tag{11}$$

where

$$H_{\alpha\alpha} = \sum_{j<k} D_{jk}(3I_{\alpha j}I_{\alpha k} - \mathbf{I}_j\cdot\mathbf{I}_k)\,, \quad \alpha = x,y,z\,, \tag{12}$$

and that each dipolar coupling constant $D_{jk}$ depends on the length and orientation of the internuclear vector joining spins $j$ and $k$.

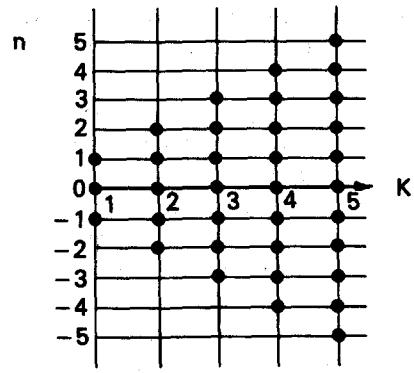


FIG. 1. Projection of Liouville space onto a two-dimensional plane. Each point represents a family of $K$-spin/$n$-quantum coherences.

The allowed pathways in Liouville space, hence the selection rules, follow from the evaluation of all coefficients $\Omega_{Knp;K'n'p'}$ according to Eq. (A7), using the Hamiltonian (10) and the commutation relations

$$[I_z, I_\pm] = I_\pm \tag{13a}$$

and

$$[I_+, I_-] = 2I_z\,. \tag{13b}$$

The result for each pair of spins,

$$(Knp|\hat{H}_{jk}|K'n'p') = \delta_{K,K\pm1}\delta_{n,n\pm2}\,, \tag{14}$$

where $|n| \leqslant K$ and $K \geqslant 1$, shows that $H_{yx}$ acts both to increase or decrease the order of coherence by two units and to add or subtract one spin to the cluster among which the coherence is shared. The clustering process is limited by the requirement that the absolute value of $n$ must not exceed $K$. A "road map" of the Liouville space then may be constructed on the basis of these rules once the starting point is specified. The routes open to a system of six spins initially in thermal equilibrium in high field and at high temperature, where the reduced density operator $\rho(0)$ is proportional to $I_z$ ($K = 1$, $n = 0$), are illustrated in Fig. 2 as an example. Only the upper half-plane ($n \geqslant 0$) is shown since the pathways are symmetric about the $K$ axis; owing to this degeneracy, the problem may be simplified accordingly, provided that the substitution $n \to |n|$ is always implicit. With a different starting point, say $\rho(0)$ proportional to $I_x$ or $I_y$ ($K = 1, n = |1|$), the same selection rules lead to the development only of odd-order coherence, i.e., $|n| = 1, 3, 5, \ldots$, rather than of even-order coherence.

We note in passing that Fig. 2 clearly shows that four-quantum coherence will not develop in a four-spin system initially in equilibrium and then subject to $H_{yx}$, an observation made in other studies as well.[4(b),12] Selection rules for other Hamiltonians, however, such as $H_{xx}$ or $H_{yy}$, permit the

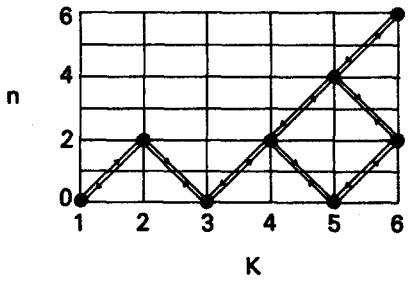


FIG. 2. Pathways in Liouville space open to a system of six spins evolving under the double-quantum Hamiltonian $H_{yx}$. Liouville states for which $\Delta K = \pm 1$ and $\Delta n = \pm 2$ are connected under this Hamiltonian. In general, if $N$ spin-1/2 nuclei initially are in thermal equilibrium, where (in the high temperature approximation) the reduced density operator is proportional to $I_z$ ($K = 1$, $n = 0$), then all even orders of coherence, up to $N$, may develop with time. Pathways are symmetric about the $K$ axis.

formation of four-quantum coherence among four spins (see Appendices B and C).

### 2. Hopping rates

At this point, the equation of motion under $H_{yx}$ may be brought into the form (9) by taking

$$\frac{d}{dt} g_{Kn}(t) = \sum_{\substack{K' = K \pm 1 \\ n' = n \pm 2}} \Gamma_{K'n';Kn} g_{K'n'}(t) - \Gamma_{Kn;K'n'} g_{Kn}(t) , \tag{15}$$

where

$$\Gamma_{Kn;K \pm 1,n \pm 2} = \frac{\Sigma_{j<k} \Sigma_{p,p'} |D_{jk}| \cdot |(Knp|\hat{H}_{jk}|K \pm 1,n \pm 2,p')|}{(Kn|Kn)} \tag{16}$$

and

$$(Kn|Kn) = \sum_{p} (Knp|Knp) . \tag{17}$$

Thus each of the four potential routes into and each of the four potential routes out of every accessible point in Liouville space is governed by an appropriate coefficient $\Gamma$, which sets the rate of flow. In general, the expression (16) is still too complex to solve, but a considerable simplification can be effected if the complicated, and possibly unknown, spectrum of coupling constants $D_{jk}$ is removed from the summation to yield

$$\Gamma_{Kn;K \pm 1,n \pm 2} = W_{Kn;K \pm 1,n \pm 2} \cdot S_1 , \tag{18}$$

where

$$W_{Kn;K \pm 1,n \pm 2} = \frac{\Sigma_{j<k} \Sigma_{p,p'} |(Knp|\hat{H}_{jk}|K \pm 1,n \pm 2,p')|}{(Kn|Kn)} \tag{19}$$

and where $S_1$ is a quantity that depends on the structure of the material. There are no absolute guidelines for constructing the parameter $S_1$, but its form should reflect the coupling constants associated with a particular system. We may, for example, take a lattice sum of the coupling constants, so that

$$S_1 = \frac{1}{N} \sum_{j<k} |D_{jk}| , \tag{20}$$

or, alternatively, we may simply take $S_1$ as proportional to the dipolar linewidth. Although such an *ad hoc* rearrangement is a drastic departure from the exact form, it is entirely in keeping with the "thermodynamic" spirit of the hopping model. Now the exchange between any two accessible sites in Liouville space is viewed as proceeding at a rate determined by the degeneracy of the coherences in question, and is scaled uniformly by just one structural parameter. Therefore, within this approximation the behavior of all large spin systems is universal: the rates depend on a material property, but the general patterns of development are the same. Since all large systems tend to look alike, the units of time can always be scaled in such a fashion. This assumption is supported experimentally, to some extent, by studies of multiple-quantum dynamics in solid solutions.[11]

To evaluate the hopping rate $W_{Kn;K \pm 1,n \pm 2}$, we first examine the scalar product $(Kn|Kn)$ appearing in the denominator of the defining expression (19). This scalar product, reflecting the degeneracy of the Liouville state $|Kn)$, is the total number of ways of realizing $n$-quantum coherence from $K$ spins-$\frac{1}{2}$. In each instance there will be $c_+$ single-spin operators $I_+$, $c_-$ single-spin operators $I_-$, and $c_0$ single-spin operators $I_z$ in the product term. Note that $c_+$ and $c_-$ sum to $n$ and that $c_+$, $c_-$, and $c_0$ sum to $K$, so that $c_0$ is not independent. For a given selection of $c_+$ and $c_-$, there are then $\binom{K}{c_+}$ $[\equiv K!/c_+!(K-c_+)!]$ different ways of choosing $c_+$ spins out of $K$ and $\binom{K-c_+}{c_-}$ different ways of choosing $c_-$ spins out of the remaining $K - c_+$, for a total of $\binom{K}{c_+} \cdot \binom{K-c_+}{c_-}$ possibilities. The full set is obtained by summing over all admissible values of $c_+$, beginning with $c_+ = n$, and multiplying the total by the factor $\binom{N}{K}$, the number of ways of selecting a subset of $K$ spins from $N$. The result is

$$(Kn|Kn) = \binom{N}{K} Q_{Kn} , \tag{21}$$

where

$$Q_{Kn} = \sum_{c=|n|}^{c_{\max}} \binom{K}{c} \binom{K-c}{c-|n|} . \tag{22}$$

According to this definition, $Q_{00} = 1$, $Q_{10} = 1$ and $Q_{KK} = 1$; moreover, $Q_{Kn} = 0$ for $n > K$. The summation is terminated when $(c - |n|)$ exceeds $(K - c)$.

Similar combinatorial arguments are used to calculate the number of ways of connecting Liouville states $|Kn)$ and $|K \pm 1,n \pm 2)$, by which is determined the numerator of Eq. (19). The final expressions are

$$W_{Kn;K+1,n \pm 2} = \frac{K(N-K)}{N-1} \cdot \frac{Q_{K-1,n} + Q_{K-1,n \pm 1}}{Q_{Kn}} \tag{23a}$$

and

$$W_{K+1,n \pm 2;Kn} = \frac{K(K+1)}{N-1} \cdot \frac{Q_{K-1,n} + Q_{K-1,n \pm 1}}{Q_{K+1,n \pm 2}} , \tag{23b}$$

with $Q_{Kn}$ as defined above in Eq. (22).

We see immediately from these expressions that moves forward, to increasing $K$, are distinguished from moves backward by the prefactors $K(N-K)/(N-1)$ and

TABLE I. Hopping rates for six spins under $H_{yx}$.

| $K$ | $n$ | $K'$ | $n'$ | $W_{Kn;K'n'}$ |
|---|---|---|---|---|
| 1 | 0 | 2 | 2 | 1.000 00 |
| 2 | 2 | 1 | 0 | 0.400 00 |
| 2 | 2 | 3 | 0 | 1.600 00 |
| 3 | 0 | 2 | 2 | 0.171 43 |
| 3 | 0 | 4 | 2 | 1.285 71 |
| 4 | 2 | 3 | 0 | 1.200 00 |
| 4 | 2 | 5 | 0 | 1.440 00 |
| 5 | 0 | 4 | 2 | 0.705 88 |
| 5 | 0 | 6 | 2 | 0.686 28 |
| 6 | 2 | 5 | 0 | 2.333 33 |
| 4 | 2 | 5 | 4 | 0.640 00 |
| 5 | 4 | 4 | 2 | 3.200 00 |
| 5 | 4 | 6 | 2 | 1.000 00 |
| 6 | 2 | 5 | 4 | 0.333 33 |
| 5 | 4 | 6 | 6 | 0.200 00 |
| 6 | 6 | 5 | 4 | 6.000 00 |

$K(K+1)/(N-1)$, respectively. Hence for very large $N$ and relatively small $K$, the reverse rates are zero and the forward rates are on the order of $K$. Consequently in a homogeneous solid, where $N$ is effectively infinity, there will be an overwhelming tendency to correlate larger and larger numbers of spins until $K$ approaches $\sqrt{N}$, at which point reverse moves become probable. When $K$ nears $N$, forward motion slows and the reverse rates go as $K$ in the limit that $N\rightarrow\infty$. In this way a balance between forward and reverse moves is always maintained, regardless of the true size of the system. Eventually any assembly of coupled spins, however large, will exhibit the characteristics of a bounded system.

Hopping rates for a six-spin system under $H_{yx}$ are listed in Table I in order to convey some idea of the details of the exchange processes. Rates for other Hamiltonians are derived in Appendix C.

### *3. Solution of the rate equations*

The final set of rate equations is familiar from many other physical problems, and naturally can be solved by standard methods. It is convenient to assign a serial number to each occupied point in Liouville space (e.g., $|K=1,n=0)\equiv 1$, $|K=3,n=0)\equiv 2$, $|K=5,n=0)\equiv 3$, etc.) and form a column vector $\mathbf{g}(t)$ and rate matrix $\mathbf{R}$ as in Eq. (9). Laplace transformation of Eq. (9) then yields

$$\mathbf{g}(s)=(s\mathbf{1}-\mathbf{R})^{-1}\mathbf{g}(t=0)\,, \tag{24}$$

where $s$ is the complex variable in the transformation. Solution of Eq. (24) is facilitated by diagonalizing the rate matrix via the similarity transform

$$\mathbf{R}_D=\mathbf{Z}^{-1}\mathbf{R}\mathbf{Z} \tag{25}$$

to find the eigenvalues $\lambda(=\lambda_1,\lambda_2,\ldots)$.[18] Use of the identity $\mathbf{Z}\mathbf{Z}^{-1}=\mathbf{1}$ in Eq. (24) eventually gives the simpler form

$$g_i(s)=\sum_j \frac{Z_{ij}}{s-\lambda_j}\sum_k Z_{jk}^{-1}g_k(0) \tag{26}$$

for each component, since $\mathbf{Z}$ diagonalizes $(s\mathbf{1}-\mathbf{R})$ as well. Application of the Laplace inversion formula to this last expression yields the desired result:

$$g_i(t)=\sum_j \exp(\lambda_j t)Z_{ij}\sum_k Z_{jk}^{-1}g_k(0)\,. \tag{27}$$

Analytical solutions are readily obtained for small systems, but in general the problem must be solved numerically. The results reported in the next section were obtained on an IBM 3081G, using IMSL subroutines for the matrix diagonalization and inversion. Double-precision arithmetic was employed throughout.

## III. RESULTS AND DISCUSSION

### A. Development of coherence under a double-quantum Hamiltonian

If no approximations are made, then a description of the dynamics of $N$ coupled spins requires the solution of a $2^N\times 2^N$ density matrix and knowledge of up to $N(N-1)/2$ dipole–dipole coupling constants. Therefore for systems of 6, 21, and 40 spins, we begin with 4096, $4.4\times 10^{12}$, and $1.2\times 10^{24}$ matrix elements, respectively, and as many as 780 coupling constants. Under the assumptions of the hopping model, however, the linear dimension of the rate matrix, equal to the total number of sites visited as the coherences migrate through Liouville space, is 8 for the case $N=6$, 66 for the case $N=21$, and 220 for the case $N=40$. At the same time, the full set of coupling constants is replaced by a single parameter that reflects the width of the dipolar spectrum.

Curves illustrating the predicted development of $n$-quantum coherence under $H_{yx}$ in these three systems are presented in Fig. 3. Each curve traces the combined history of all modes of a given order $n$ by showing the variation of the coherence amplitude

$$g_n(t)=\sum_K g_{Kn}(t) \tag{28}$$

with time. Prior to excitation the spins are assumed to exist in equilibrium in the high-temperature limit; during excitation the units of time are arbitrary, normalized to the inverse of the parameter $S_1$.

The course of development is qualitatively similar in all three systems, with lower orders of coherence always appearing before higher orders and with the system reaching a steady state under prolonged excitation. In each instance the amplitude of the two-quantum coherence quickly peaks and then falls off to a constant level as the excitation is maintained. Coherences of higher order develop in turn, each reaching a steady-state value of its own after sufficient time. As the total number of spins increases, the maximum in the curve $g_2(t)$ becomes more pronounced and higher orders $g_n(t)$ continue to grow in, up to approximately $n=2\sqrt{N}$. The sum of all the amplitudes, including $g_0(t)$, remains equal to unity at all times.

The need for an "induction time" to elapse before coherence of a given order is observed has been predicted in exact theoretical treatments of small systems[17] and verified experimentally in studies of anisotropic fluids and, recently, of polycrystalline solids.[9,11] The delay arises because an $n$-quantum coherence can be sustained by no fewer than $n$ spins, interdependent in a dynamical sense owing to the two-spin Hamiltonian, and because it takes time to establish the

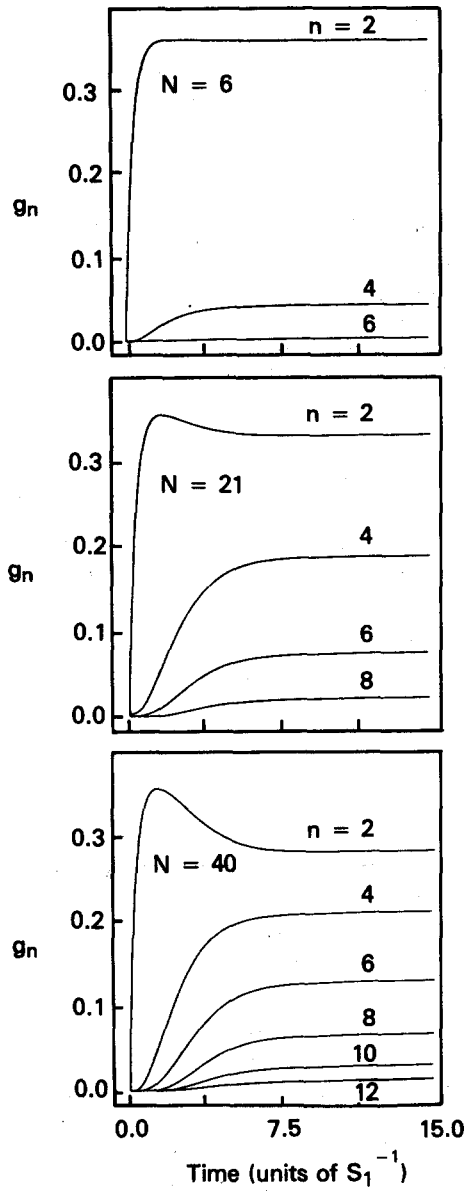


FIG. 3. Development of $n$-quantum coherence in systems of various sizes, as predicted by the hopping model. Zero-quantum coherences, not shown, begin as $g_0(0) = 1$ and decay to steady-state values. In each example the time axis is scaled to the inverse sum of the dipole–dipole coupling constants.

necessary correlations. The formal solution to the equation of motion,

$$\rho(t) = \exp(-iH_{yx}t)\rho(0)\exp(iH_{yx}t)\,, \tag{29}$$

suggests that the time required for a coupling $D_{jk}$ to propagate from spin $j$ to spin $k$ is related to the inverse rate $1/D_{jk}$; consequently, distant spins, with smaller couplings, are drawn into the network at later times. According to the hopping model, which neglects variations in the coupling constants, similar delays still must arise since the migrating coherence must travel to more distant regions of Liouville space as the order of coherence, and hence the size of the correlated cluster, increases. This point is implicit in the pathways in Fig. 2, which show that the coherences $|Kn)$ are reached sequentially, in order of increasing $K$ and $n$.

Long-term stability of multiple-quantum coherence amplitudes has been noted before in numerical simulations of the exact density operator dynamics in systems of approximately six spins.[17] Such behavior inevitably emerges when the dynamics are sufficiently complex, as we assumed originally in developing the hopping model. These observations have been used to support an earlier statistical picture in which it is assumed that, in the limit of long excitation times, all coherence amplitudes have the same magnitude but random phases. In this view the contribution of an $n$-quantum coherence, reflected by the integrated intensity of the $n$-quantum spectrum, is proportional to the number of pairs of states differing by $n$ units in the Zeeman quantum number. Combinatorial arguments then predict a Gaussian distribution,

$$g_n(\infty) \propto \exp(-n^2/N)\,, \quad n>0\,, \tag{30}$$

for the $n$-quantum coherence after a steady state is attained.[17] Precisely the same results are obtained with the hopping model, which takes a statistical view of the development at all times: the limiting values of all coherences $g_n$ plotted in Fig. 3 are well fit by the Gaussian distributions above with $N = 6$, 21, and 40.

In Fig. 4, the theoretical predictions for $g_n(t)$ are compared with existing multiple-quantum intensity data for 6 and 21 spins excited under $H_{yx}$.[12] The smaller system is actually a dilute solid solution consisting of guest molecules with six protons in a perdeuterated host, so the simple picture of six spins, valid for short excitation times, may change as the excitation is prolonged. The larger system is a molecule with 21 spins, oriented in a nematic phase, and is a realistic example of an isolated cluster of finite size. To facilitate the comparison, we have normalized each curve to the intensity of the entire multiple-quantum spectrum ($n>0$), plotting $g_n(t)/[g_2(t)+g_4(t)+\cdots]$ vs time in units of reciprocal $S_1$. These experimental results, which match the important features of the generic theoretical curves both at short and long times, lend support to the basic assumptions used to construct the hopping model.

Multiple-quantum dynamics in infinitely extended systems, such as dipolar solids, can be understood only by studying finite systems of increasing size, for the complete rate matrix from $K = 1$ to $K = N$ must always be used. When $N$ is large, the rates for the reverse moves $K \to K-1$ are vanishingly small except as $K$ approaches $N$. If the rate matrix is truncated at $K < N$, the coherences will move towards the highest value of $K$ considered—at which point they are trapped, unable to go back because the rate is too low and unable to go forward because of the arbitrary cutoff. With the detailed balance of the system thus destroyed, the rate equations typically cannot be solved, and even when they can be solved, the solution is without physical meaning. Consequently, to model the dynamics in a solid we need to extrapolate the trends observed in smaller systems. We can reasonably predict that low orders of coherence will peak and then fall off to a limiting value, and that higher orders of coherence will grow in more slowly without necessarily exhibiting local maxima. If the system is in fact infinite, then at very long times all coherence amplitudes should reach the same level. These expectations are confirmed in Fig. 5,

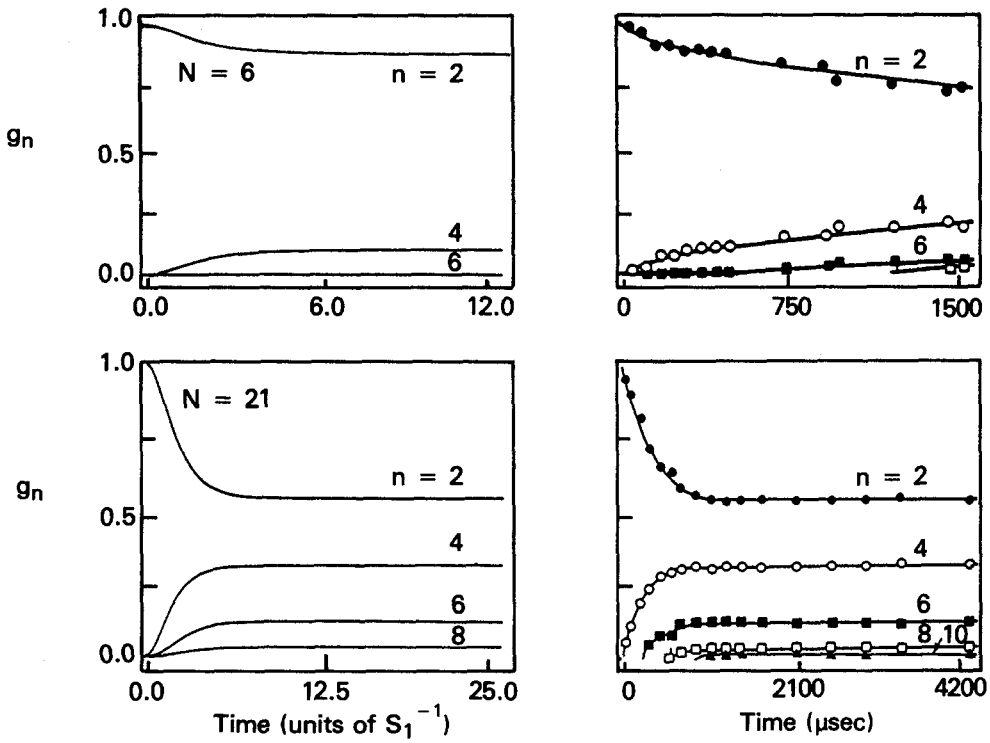


FIG. 4. Development of $n$-quantum coherence within isolated groups of 6 and 21 spins, predicted theoretically (left) and measured experimentally (right). Each point is normalized to the total spectral intensity excluding zero-quantum contributions. The experimental results are for a dilute solid solution of a molecule with 6 $^1$H nuclei in a deuterated host (top) and for a molecule with 21 $^1$H nuclei in a nematic phase (bottom). The different time scales reflect differences in structure and molecular motion between the two materials. For the 6-spin system, 12 units of "theoretical" time correspond to 1500 $\mu$s of experimental excitation time; whereas for the 21-spin system, 25 units of theoretical time correspond to 4200 $\mu$s of real time. Agreement is excellent in the case of the liquid crystal, where averaging of intermolecular dipole–dipole interactions effectively isolates the molecules. Coupling between guest molecules in the solid solution, however, ultimately increases the effective cluster size beyond 6. (Experimental data courtesy of J. Baum.[12])

where previously reported experimental multiple-quantum intensity data for polycrystalline hexamethylbenzene are reproduced.[11] Curves for $n = 4$, 8, 12, and 16 are shown, and the shapes, if not the coherence orders, are similar to those in each part of Fig. 3. The distribution of coherence after 600–700 $\mu$s is consistent with an effective cluster size of several hundred spins, so it is not surprising that $g_4(t)$ reaches a maximum and that all curves $g_n(t)$ appear to approach the same value.

### B. Development of clusters of correlated spins

To follow the formation of interparticle correlations under a two-spin Hamiltonian such as $H_{yx}$, we now consider the quantity

$$g_K(t) = \sum_n g_{Kn}(t) , \tag{31}$$

the sum of all coherence amplitudes derived from a cluster of $K$ spins. This combined amplitude provides a measure of the growth of a network of $K$ spins within which coherences from $n = 0$ to $n = K$ may develop.

Curves illustrating the predicted development of $K$-spin coherence (for $K = 2$, 13, and 20) in a system of 21 spins are shown in Fig. 6. Two important features are immediately apparent. First, clusters of increasing size appear at increasing times, as expected; and second, coherence originating from small clusters peaks early and then falls off, while coherence originating from large clusters reaches a plateau as

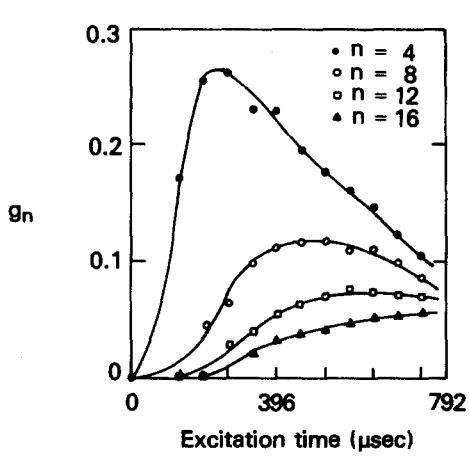


FIG. 5. $^1$H multiple-quantum intensity in polycrystalline hexamethylbenzene, measured for increasing excitation times. Smooth curves have been drawn through the points. The general pattern of coherence development in this unbounded system is similar to that predicted in Fig. 3 for groups of finite sizes. (Reprinted from Ref. 11.)

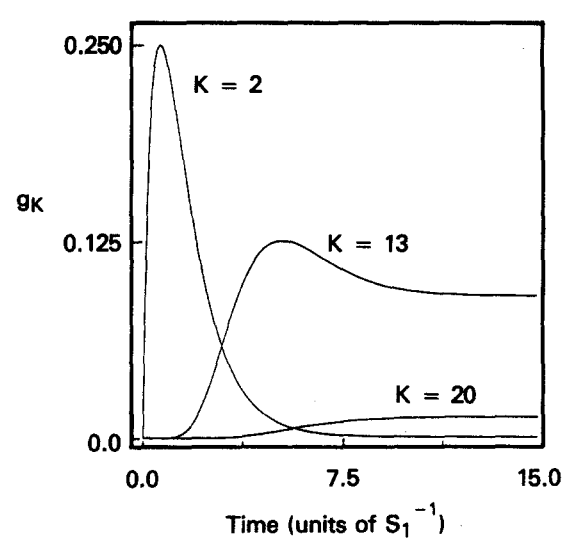


FIG. 6. Formation of $K$-spin coherence within a group of 21 spins, according to the hopping model. Larger clusters contribute to the spin dynamics at later times.

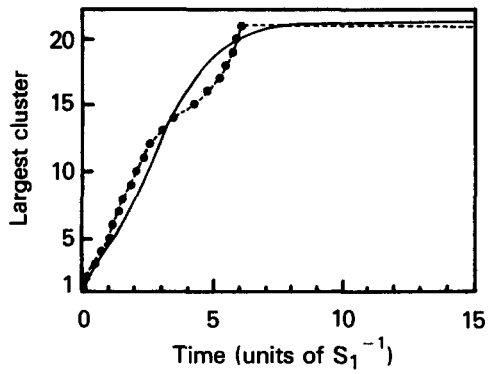


FIG. 7. Variation of the effective size of the system with time under $H_{yx}$. The points connected by the broken line give the induction time $t_K$ associated with each $K$-spin coherence. The solid line results from fitting the calculated $n$-quantum intensities to the function $\exp(-n^2/K_{\max})$. In each view, the largest cluster approaches $N$ ( = 21) spins after prolonged excitation.

time passes. An induction time $t_K$, defined as the time needed for $g_K(t)$ to reach half its maximum value, therefore can be associated with each cluster. A point-to-point plot of $K$ vs $t_K$, connected by a broken line, is presented in Fig. 7 to show how the 21 spins, initially uncoupled, eventually become completely interdependent as the correlations develop. The network formed in this way widens with time and ultimately encompasses all $N$ spins, at which point the system is dynamically "mature" and thereafter the effective size $K_{\max}$ remains equal to the true size $N$.

Hence at any time there exist independent clusters ranging from 1 to $K_{\max}$ correlated spins, with the largest cluster defining the instantaneous effective size of the system. The simplest approximation for $K_{\max}$, made in previous studies, follows from assuming a Gaussian distribution of $n$-quantum coherence.[11] According to this view, $K_{\max}$ then may be obtained by fitting an observed (or calculated) distribution of multiple-quantum spectral intensity to Eq. (30). The picture is tantamount to assuming that the system is always in the long-term statistical limit, admittedly a chancy proposition when the effective size is still increasing but one that yields reasonably consistent results nonetheless. To explore this idea, we first calculate the values of $K_{\max}$ that result from assuming that the $n$-quantum coherence amplitudes $g_n(t)$ predicted by the hopping model can be fit to a Gaussian, and then examine the growth in $K_{\max}$ over time. Some idea of the quality of the fit is conveyed in Fig. 8, where the calculated amplitudes for $N = 21$ are compared with the values $\exp[-n^2/K_{\max}(t)]$ obtained by extracting a time-dependent effective size from the same calculated amplitudes according to Eq. (30). Even when $K_{\max}$ is significantly less than $N$, the computed intensities are reasonably well described by a simple Gaussian, subject to the usual underestimation of the contributions from the highest orders of coherence.[17] In Fig. 7 the solid line shows how $K_{\max}$ changes with time, steadily increasing up to the true size $N$ and then leveling off. Comparing the two curves, we see that the behavior predicted by the hopping model, although certainly not described by a simple time dependence, roughly tracks the behavior predicted by the model of an expanding system always in the statistical limit. In particular, the system matures at the same time, and, when smoothed, the early time development is remarkably similar in both pictures. This basic agreement is critical if multiple-quantum intensities are to be used to determine the extent of real spin clusters in various materials.

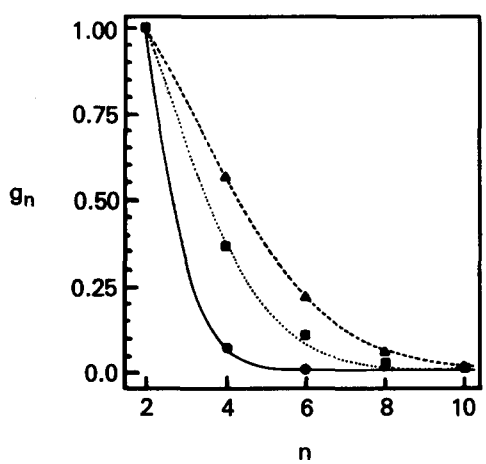


FIG. 8. Plots of $g_n$ vs $n$, normalized to $g_2$, for three excitation times in a system of 21 spins. The points give the values of $g_n/g_2$ predicted by the hopping model, and the curves show the best fit of these data to a Gaussian distribution. Times were selected to obtain $K_{\max} \sim 4$ (solid line), 12 (dotted line), and 21 (dashed line).

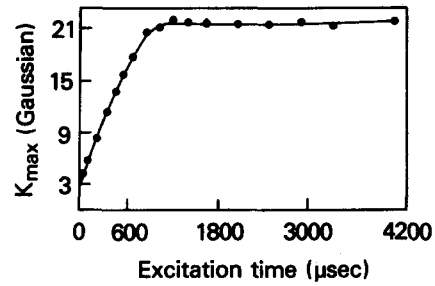


FIG. 9. Largest cluster of correlated spins vs excitation time for the nematic system of Fig. 4, computed by fitting measured multiple-quantum intensities to a Gaussian distribution. The pattern observed is virtually identical to that shown in Fig. 7. For the relationship between real time and theoretical time, see Fig. 4. (Courtesy of J. Baum.[12])

For comparison, values of the time-dependent effective size measured in the 21-spin system studied in Ref. 12 are reproduced in Fig. 9. Each point has been obtained by fitting the experimentally observed multiple-quantum intensities shown in Fig. 4 to the Gaussian (30), and the curve that results agrees very satisfactorily with the pattern predicted in Fig. 7.

### C. Nonequilibrium initial conditions

We now briefly consider the development of multiple-quantum coherence in systems initially out of equilibrium, taking as a first example the case $N = 6$ with the eight Liouville states accessible under $H_{yx}$ equally populated before excitation begins. Under these conditions $n$-quantum coherence develops as in Fig. 10 rather than as in Fig. 3. The initial nonequilibrium distribution $g_{Kn}(0) = 1/8$ (for the eight points shown in Fig. 2) evolves, however, to the same steady-state distribution $g_n \sim \exp(-n^2/N)$ reached by a system

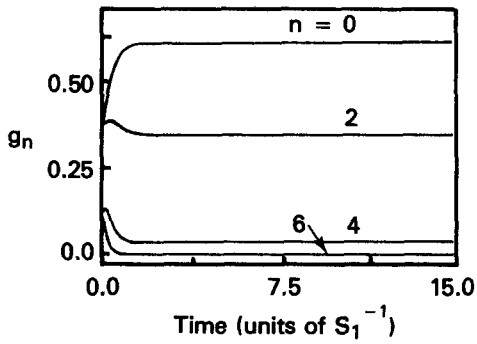


FIG. 10. Development of $n$-quantum coherence as predicted by the hopping model for six spins not initially in equilibrium. Initial conditions are $g_{Kn} = 1/8$ for each of the eight points shown in Fig. 2, so that $g_0(0) = g_2(0) = 0.375$ and $g_4(0) = g_6(0) = 0.125$. After some time the system follows the same course as one beginning in thermal equilibrium.

originally in thermal equilibrium, i.e., where $g_{1,0}(0) = 1$. A similar result is also obtained for other nonequilibrium initial conditions—for example, six-quantum coherence. Note that in these circumstances the notion of a Gaussian distribution of coherence intensities, as well as the notion of a continuously increasing effective size, becomes meaningless.

The hopping model, by positing a set of exponential solutions to the Liouville–von Neumann equation, may predict curiously unphysical behavior given certain nonequilibrium initial conditions. For example, if $\rho(0)$ is proportional to one of the eigenstates of the rate matrix, denoted by $u(0)$, then the solution to Eq. (9) is

$$\mathbf{u}(t) = \exp(\lambda t)\mathbf{u}(0)\,, \tag{32}$$

where $\lambda$ is the corresponding eigenvalue. Under these conditions the density operator either decays to zero or diverges with time, depending on whether the eigenvalue is negative or positive. This difficulty poses no serious challenge to the hopping model in practice, however, for the initial conditions required to bring out such behavior are unlikely to be attained.

## IV. SUMMARY

The approach described in this paper provides a general framework for understanding spin dynamics in systems too large or too complicated to be treated exactly. In these systems the Liouville–von Neumann equation for the density operator is replaced by a set of rate equations with exponential rather than oscillatory solutions, in recognition of the severe damping that inevitably accompanies the superposition of a large number of independent frequency components. The equations that result then can be solved straightforwardly for groups of spins of various sizes. According to this picture, the evolution of the density operator is viewed as a series of discrete hops in Liouville space, with the selection rules determined by the commutation properties of the Hamiltonian. For the pure double-quantum Hamiltonian $H_{yx}$, each move takes the system from a $K$-spin/$n$-quantum mode to a $(K \pm 1)$-spin/$(n \pm 2)$-quantum mode. The rate for going from one point in Liouville space to another depends on both the number of Liouville states with quantum numbers $K$, $n$, $K \pm 1$, and $n \pm 2$ at each end and on the magnitude of the effective cluster size $K$ relative to the true size of the system $N$. The model shows that, except when $K$ approaches $N$, the rates for the reverse pathways (decreasing $K$), vanish for infinitely extended systems such as dipolar solids, but that all pathways are allowed when $N$ is finite. Overall, the jump rates are uniformly scaled by some quantity that depends on the properties of the material, such as the dipolar linewidth, but otherwise the behavior predicted is universal. The same approach can be taken for other phenomena—for example, the problem of relaxation of multiple-quantum coherence under a secular dipolar Hamiltonian. Less drastic approximations can of course be introduced, although some of the simplicity of the present model will undoubtedly be lost by so doing. Extensions of this sort will be discussed in future reports.

## ACKNOWLEDGMENTS

We thank J. Baum for kindly providing the experimental data reproduced in Figs. 4 and 9 prior to publication. M. Mehring acknowledges several intense, informative discussions with A. N. Garroway in the early stages of this work. M. Munowitz acknowledges a useful discussion with D. J. Vezzetti. This research was supported in part by NATO, through grant no. 202/81, and by the Director, Office of Energy Research, Office of Basic Energy Sciences, Materials Science Division of the U. S. Department of Energy under contract DE-AC03-76SF00098.

## APPENDIX A: LIOUVILLE STATES FOR $N$ COUPLED SPINS

Using the single-spin spherical tensor operators

$$T_{0j} \equiv I_{zj}, \quad T_{+j} \equiv \frac{-1}{\sqrt{2}} I_{+j}, \quad \text{and} \quad T_{-j} \equiv \frac{1}{\sqrt{2}} I_{-j}\,, \tag{A1}$$

we construct orthonormal Liouville states

$$|s_1\alpha_1 \cdots s_K\alpha_K) \equiv 2^K 2^{-N/2} |T_{s_1\alpha_1} \cdots T_{s_K\alpha_K})\,, \tag{A2}$$

such that

$$(t_K\beta_K \cdots t_1\beta_1 | s_1\alpha_1 \cdots s_K\alpha_K) = \delta_{s_1t_1}\delta_{\alpha_1\beta_1} \cdots \delta_{s_Kt_K}\delta_{\alpha_K\beta_K}\,. \tag{A3}$$

In the above expression, the scalar product of two operators $A$ and $B$ is defined as

$$(A\,|B) \equiv \mathrm{Tr}\{A^\dagger B\}\,, \tag{A4}$$

where $A^\dagger$ is the adjoint of $A$. To emphasize that each Liouville state is formed as a product of $K$ single-spin operators whose combined action is responsible for an $n$-quantum coherence, we use the abbreviated notation

$$|Knp) \equiv |s_1\alpha_1 \cdots s_K\alpha_K)\,, \tag{A5}$$

where

$$n = \sum_{j=1,K} \alpha_j\,. \tag{A6}$$

The parameter $p$ labels the various states with given values of $K$ and $n$.

Matrix elements involving the superoperator $\hat{H}$ are defined as

$$\langle A|\hat{H}|B\rangle \equiv \mathrm{Tr}\{A^{\dagger}[H,B]\}. \tag{A7}$$

## APPENDIX B: FORMS OF THE DIPOLE–DIPOLE HAMILTONIAN

Dipole–dipole Hamiltonians of different symmetries can appear as average Hamiltonians in multiple-pulse NMR experiments. All these operators can be condensed into the form

$$H_{\alpha\beta} = \sum_{j<k} D_{jk} H_{\alpha\beta}^{(jk)}, \quad \alpha,\beta = x,y,z, \tag{B1}$$

where

$$H_{\alpha\alpha}^{(jk)} = 3I_{\alpha j}I_{\alpha k} - \mathbf{I}_j\cdot\mathbf{I}_k. \tag{B2}$$

In terms of the raising and lowering operators, we have

$$H_{xx}^{(jk)} = -I_{zj}I_{zk} + \tfrac{1}{4}(I_{-j}I_{+k} + I_{+j}I_{-k}) + \tfrac{3}{4}(I_{+j}I_{+k} + I_{-j}I_{-k}), \tag{B3}$$

$$H_{yy}^{(jk)} = -I_{zj}I_{zk} + \tfrac{1}{4}(I_{-j}I_{+k} + I_{+j}I_{-k}) - \tfrac{3}{4}(I_{+j}I_{+k} + I_{-j}I_{-k}), \tag{B4}$$

$$H_{zz}^{(jk)} = 2I_{zj}I_{zk} - \tfrac{1}{2}(I_{+j}I_{-k} + I_{-j}I_{+k}), \tag{B5}$$

and the combination

$$H_{yx}^{(jk)} = \tfrac{1}{3}[H_{yy}^{(jk)} - H_{xx}^{(jk)}] = -\tfrac{1}{2}(I_{+j}I_{+k} + I_{-j}I_{-k}). \tag{B6}$$

Note that $H_{yx}$ contains only the two-quantum operators $I_{+j}I_{+k}$ and $I_{-j}I_{-k}$, and that the "natural" Hamiltonian $H_{zz}$ contains only the zero-quantum operators $I_{+j}I_{-k}$ and $I_{-j}I_{+k}$. In contrast, $H_{xx}$ and $H_{yy}$ contain both zero-quantum and two-quantum terms.

## APPENDIX C: HOPPING RATES IN LIOUVILLE SPACE UNDER VARIOUS HAMILTONIANS

Hopping rates $\Gamma$ were defined in the text as

$$\Gamma_{Kn;K\pm1,n\pm2} = W_{Kn;K\pm1,n\pm2}\cdot S_1, \tag{C1}$$

where the universal factor

$$W_{Kn;K\pm1,n\pm2} = \frac{\Sigma_{j<k}\,\Sigma_{p,p'}|(Knp|\hat{H}_{jk}|K\pm1,n\pm2,p')|}{(Kn|Kn)} \tag{C2}$$

establishes the basic rate and where $S_1$ is a parameter dependent on the specific set of dipolar coupling constants—for example, the lattice sum

$$S_1 = \frac{1}{N}\sum_{j<k}|D_{jk}|. \tag{C3}$$

In this Appendix we give expressions for $W_{Kn;K'n'}$ under different Hamiltonians.

(1) $H_{zz}(\Delta n = 0)$:

$$W_{Kn;K+1,n} = \frac{K(N-K)}{N-1}\cdot\frac{2Q_{K-1,n} + 3Q_{K-1,n-1} + 3Q_{K-1,n+1}}{Q_{Kn}}, \tag{C4}$$

$$W_{K+1,n;Kn} = \frac{K(K+1)}{N-1}\cdot\frac{2Q_{K-1,n} + 3Q_{K-1,n-1} + 3Q_{K-1,n+1}}{Q_{K+1,n}}, \tag{C5}$$

(2) $H_{xx},H_{yy}(\Delta n = 0)$:

$$W_{Kn;K+1,n} = \frac{K(N-K)}{2(N-1)}\cdot\frac{2Q_{K-1,n} + 3Q_{K-1,n-1} + 3Q_{K-1,n+1}}{Q_{Kn}}, \tag{C6}$$

$$W_{K+1,n;Kn} = \frac{K(K+1)}{2(N-1)}\cdot\frac{2Q_{K-1,n} + 3Q_{K-1,n-1} + 3Q_{K-1,n+1}}{Q_{K+1,n}}. \tag{C7}$$

Note that these rates are exactly half the corresponding expressions for $H_{zz}$.

(3) $H_{xx},H_{yy}(\Delta n = \pm 2)$:

$$W_{Kn;K+1,n\pm2} = \frac{3K(N-K)}{2(N-1)}\cdot\frac{Q_{K-1,n} + Q_{K-1,n\pm1}}{Q_{Kn}}, \tag{C8}$$

$$W_{K+1,n\pm2;Kn} = \frac{3K(K+1)}{2(N-1)}\cdot\frac{Q_{K-1,n} + Q_{K-1,n\pm1}}{Q_{K+1,n\pm2}}. \tag{C9}$$

(4) $H_{yx}$ $(\Delta n = \pm 2)$:

$$W_{Kn;K+1,n\pm2} = \frac{K(N-K)}{N-1}\cdot\frac{Q_{K-1,n} + Q_{K-1,n\pm1}}{Q_{Kn}}, \tag{C10}$$

$$W_{K+1,n\pm2;Kn} = \frac{K(K+1)}{N-1}\cdot\frac{Q_{K-1,n} + Q_{K-1,n\pm1}}{Q_{K+1,n\pm2}}. \tag{C11}$$

$Q_{Kn}$ is defined as

$$Q_{Kn} = \sum_{c=|n|}^{c_{\max}}\binom{K}{c}\binom{K-c}{c-|n|}, \tag{C12}$$

with $0\leqslant|n|\leqslant K$ and $Q_{00} = Q_{10} = Q_{KK} = 1$.

[1] (a) U. Fano, Rev. Mod. Phys. **29**, 74 (1957); (b) S. Vega, J. Chem. Phys. **68**, 5518 (1978); (c) A. Wokaun and R. R. Ernst, *ibid.* **67**, 1752 (1977).
[2] O. W. Sørensen, G. W. Eich, M. H. Levitt, G. Bodenhausen, and R. R. Ernst, Progr. NMR Spectrosc. **16**, 163 (1983).
[3] W. P. Aue, E. Bartholdi, and R. R. Ernst, J. Chem. Phys. **64**, 2229 (1976).

[4](a) G. Bodenhausen, Progr. NMR Spectrosc. **14**, 137 (1981); (b) D. P. Weitekamp, Adv. Magn. Reson. **11**, 111 (1983); (c) M. Munowitz and A. Pines, Adv. Chem. Phys. **66**, 1 (1987); (d) A. Pines, Lectures on Pulsed NMR, 100th Fermi School on Physics, Varenna, 1986 (in press), and references therein..
[5]G. Drobny, A. Pines, S. Sinton, D. P. Weitekamp, and D. Wemmer, Faraday Symp. Chem. Soc. **13**, 49 (1979).
[6]W. S. Warren, D. P. Weitekamp, and A. Pines, J. Chem. Phys. **73**, 2084 (1980).
[7]W. S. Warren and A. Pines, J. Chem. Phys. **74**, 2808 (1981).
[8]S. Sinton and A. Pines, Chem. Phys. Lett. **76**, 263 (1980); S. W. Sinton, D. B. Zax, J. B. Murdoch, and A. Pines, Mol. Phys. **53**, 333 (1984).
[9]Y.-S. Yen and A. Pines, J. Chem. Phys. **78**, 3579 (1983).
[10]A. N. Garroway, J. Baum, M. G. Munowitz, and A. Pines, J. Magn. Reson. **60**, 337 (1984).
[11]J. Baum, M. Munowitz, A. N. Garroway, and A. Pines, J. Chem. Phys. **83**, 2015 (1985).
[12]J. Baum and A. Pines, J. Am. Chem. Soc. **108**, 7447 (1986).
[13]J. Baum, K. Gleason, J. Reimer, A. Garroway, and A. Pines, Phys. Rev. Lett. **56**, 1377 (1986).
[14]P.-K. Wang and C. P. Slichter, Phys. Rev. Lett. **53**, 82 (1984).
[15]I. J. Lowe and R. E. Norberg, Phys. Rev. **107**, 46 (1957).
[16]J. Jeener, Adv. Magn. Reson. **10**, 1 (1982), and references therein.
[17]J. B. Murdoch, W. S. Warren, D. P. Weitekamp, and A. Pines, J. Magn. Reson. **60**, 205 (1984).
[18]R. G. Gordon and R. P. McGinnis, J. Chem. Phys. **49**, 2455 (1968).